The Vibrational Structure of the OH Radical in Solid Argon: A Transfer-Matrix Path-Integral Approach

B. J. COSTA CABRAL

Departamento de Química e Bioquímica, Faculdade de Ciências, Universidade de Lisboa, 1749-016, Lisboa, Portugal and Grupo de Física Matemática da Universidade de Lisboa, Av. Professor Gama Pinto, 2. 1649-003 Lisboa, Portugal

Received 9 January 2004; accepted 24 February 2004
Published online 6 April 2005 in Wiley InterScience (www.interscience.wiley.com).
DOI 10.1002/qua.20589

ABSTRACT: The vibrational structure of the hydroxyl radical in argon was investigated by transfer-matrix path-integral calculations. The results for the OH $X^2\Pi$ ground state in Ar indicate that the vibrational structure in the matrix is modified relative to the gas phase. However, only vibrational levels above $v = 12$ are significantly perturbed. The changes of the higher vibrational energy levels can be explained by interactions between the OH radical and the Ar matrix. We predict that the position of the OH fundamental in argon matrix is 3540 cm^{-1} in good agreement with the experimental result (3548.2 cm^{-1}). This value is red-shifted by ~6 cm^{-1} relative to the free radical (3546 cm^{-1}). In contrast with previous results for Br_2 in solid Ar, where a very large barrier related to confinement effects inhibits dissociation, the present study indicates that the OH radical can dissociate in the matrix. © 2005 Wiley Periodicals, Inc. Int J Quantum Chem 103: 610–616, 2005

Key words: vibrational structure; transfer-matrix; path-integral; solid argon; spectroscopic properties

Introduction

The hydroxyl radical (OH) has been the subject of several recent investigations, in part because OH is associated with deleterious effects on biological systems [1–4], including Parkinson's disease [5], and in atmospheric abstraction reactions the OH radical determines the lifetime of many hydrofluorocarbons [6, 7]. Herzberg's pioneering investigations on the spectroscopic properties of the OH radical [8, 9] were followed by several other studies [10–17]. As the OH radical is a very reactive species, experiments were often carried out in inert rare-gas solids, where it can be trapped. However, the characterization of the vibrational structure of the OH radical in solid argon has been a controversial issue. Acquista et al. [10] found that the $\Delta G_{1/2}$ vibrational spacing of OH ($X^2\Pi$) in the solid was red shifted by $\approx$130 cm^{-1} from its gas phase value. Goodman and Brus [11] suggested that a possible explanation for this finding was a strong interaction between the open-shell OH and the argon atoms. These authors also remarked that the shift was an order of magnitude larger than was normally observed for covalently bond molecules in rare-gas solids. Suzer and

Andrews [13] bombarded Ar/H_2O matrices with electrons; in addition to the 3452.3 cm^{-1} band, they observed the 3548.2 band, which they attributed to OH^-. Cheng et al. [12] provided further evidence that OH and OD radicals in solid argon at $T = 12$ K are characterized by their infrared absorption lines at 3548.2 and 2616.1 cm^{-1}, respectively. The first value is close to the free radical $\Delta G_{1/2}$ value of 3546 cm^{-1}, indicating a negligible interaction with the Ar matrix. Moreover, these authors indicated that although another set of lines at 3452.3 and 3428.2 cm^{-1} could be detected, the relative intensity and shapes of the lines are variable, and their presence seems to be dependent on the molar fraction of the reactants. They suggested that these lines may be attributed to OH or OD aggregates rather than to the OH radical immersed in Ar. Recently, these two lines were assigned to the ν(O—H) vibrational stretching of the radical in the H_2O—HO complex trapped at two different sites within the Ar matrix [14–16].

However, at least one relevant question deserves further investigation: How does the interaction between the OH radical and the Ar matrix modify the vibrational structure of the radical species, in particular its higher vibrational states? In the present work we report on a theoretical investigation of the OH radical vibrational properties in solid argon. Our approach is based on a mixed quantum-classical system representation for the vibrational motion (quantum degree of freedom) of the OH radical coupled to a classical system (the Ar matrix). Initially, we review the statistical theory for a mixed quantum-classical system [18, 19] and the transfer-matrix [20] path-integral [21] method [22, 23]. This is followed by a description of the potential model representing the interactions between the OH radical and Ar, which was based on second order Møller–Plesset perturbation theory calculations (MP2). Then we discuss the results for the vibrational structure of the OH radical in solid Ar and comment on possible extensions of the present procedure to the analysis of bond breaking in condensed phase.

Computational Details

MIXED QUANTUM-CLASSICAL SYSTEMS: BASIC THEORY AND TRANSFER-MATRIX PATH-INTEGRAL METHOD

The Hamiltonian for a mixed quantum-classical system can be written as [18, 19, 23]

$$H = T_f + V(r|R) + T_s + V_s(R), \quad (1)$$

where T_f and T_s are the kinetic contributions for the quantum (fast) and the classical (slow) degrees of freedom, respectively. $V(r|R)$ is defined by

$$V(r|R) = V_f(r) + V_c(r|R), \quad (2)$$

where the term $V_c(r|R)$ couples the quantum (r) and classical (R) degrees of freedom and $V_s(R)$ is the potential energy of the classical system. By assuming a Born–Oppenheimer approximation, the density matrix can be written as the product of the density matrix $\rho_f(r, r'|R)$ describing the fast degree of freedom in the configuration R of the classical variables and the density matrix ρ_s of the classical system:

$$\begin{aligned}\rho(r, R; r', R) &= Q_c \rho_f(r, r'|R) \times \rho_s(R) \\ &= Q_c \sum_n \psi_n^*(r|R)\psi_n(r'|R)\exp[-\beta E_n(R)] \\ &\quad \times \exp[-\beta V_s(R)], \quad (3)\end{aligned}$$

where Q_c is the kinetic classical partition function. Consequently, we can write the partition function for the mixed quantum-classical system as

$$Z = \int dR dr \rho(r, R; r, R) \propto \int dR \rho(R), \quad (4)$$

where

$$\rho(R) = \exp\{-\beta[V_s(R) + \mathcal{A}_q(R)]\} \quad (5)$$

and the quantum free energy $\mathcal{A}_q(R) = -\beta^{-1} \ln Z_f(R)$. Z_f is the quantum partition function given by

$$Z_f(R) = \mathrm{Tr}\ \rho_f(r, r'|R) = \int dr \rho_f(r, r|R). \quad (6)$$

For a configuration R of the classical variables, the quantum average of an observable A can be written as

$$\bar{A}(R) = [Z_f(R)]^{-1} \mathrm{Tr}(\rho_f \hat{A}). \quad (7)$$

Therefore, the canonical average of A over different configurations R can be written as

$$\langle A\rangle = [Z]^{-1}\int dR\,\exp\{-\beta[V_s(R) + \mathcal{A}_q(R)]\}\bar{A}(R). \tag{8}$$

Canonical averages can be calculated by the conventional Monte Carlo method, with the probability density given by (5). On the other hand, the quantum partition function corresponding to the quantum degree of freedom Z_f can be written in a discretized path-integral representation based on Trotter's formula:

$$Z_f(R) = \int dr_1 dr_2 \ldots dr_P (mP/2\pi\hbar^2\beta)^{P/2} \times \exp[-\beta V_{eff}(r_1, r_2, \ldots, r_P|R)], \tag{9}$$

where

$$V_{eff}(r_1, r_2, \ldots, r_P|R) = (mP/2\hbar^2\beta^2)\sum_{i=1}^{P}(r_{i+1} - r_i)^2 + (1/2P)\sum_{i=1}^{P}[V(r_i|R) + V(r_{i+1}|R)]. \tag{10}$$

Introducing the transfer-matrix for the discretization in the coordinate space $\Pi_{aa'}$ as

$$\langle a|\Pi|a'\rangle = \exp\{-\beta\{[(mP/2\hbar^2\beta)^2](a\Delta r - a'\Delta r)^2 + (1/2P)[V(a\Delta r|R) + V(a'\Delta r|R)]\}\} \tag{11}$$

Z_f can be written as

$$Z_f(R) \approx (\Delta r)^P[(mP/2\pi\hbar^2\beta)]^{P/2}\sum_{a_1}\sum_{a_2}\cdots\sum_{a_P}\langle a_1|\Pi|a_2\rangle \times \langle a_2|\Pi|a_3\rangle\cdots\langle a_P|\Pi|a_1\rangle \tag{12}$$

or

$$Z_f(R) \approx (\Delta r)^P[(mP/2\pi\hbar^2\beta)]^{P/2} \times \mathrm{Tr}\,\Pi^P = (\Delta r)^P[mP/2\pi\hbar^2\beta]^{P/2}\sum_i \lambda_i^P, \tag{13}$$

where λ_i are the eigenvalues of the matrix Π.

In the present case, the fast quantum degree of freedom corresponds to the vibrational degree of freedom of the OH radical, which is usually represented by a Morse potential. The classical system corresponds to the Ar atoms in condensed phase interacting through a Lennard-Jones potential. The quantum degree of freedom has been integrated in a 12 au interval with $\Delta r = 0.024$ au and $P = 15000$.

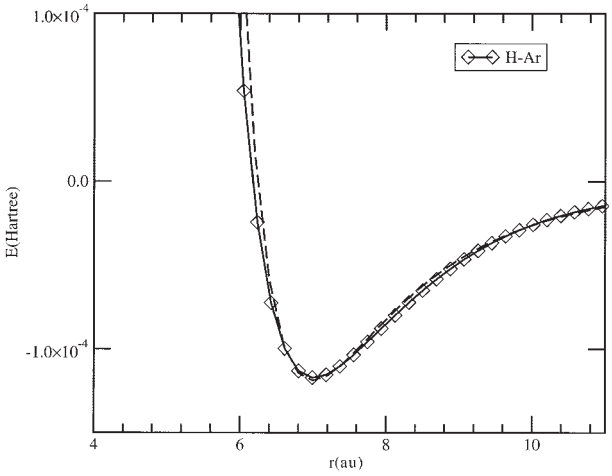

FIGURE 1. H—Ar interaction potential. UMP2/aug-cc-pVTZ calculations (diamonds) and fitted 12-6 Lennard-Jones potential (dashed curve).

AB INITIO CALCULATIONS, INTERACTION MODEL, AND MORSE POTENTIAL

Ab initio calculations using second-order Møller–Plesset perturbation theory (MP2) were carried out to study the interactions between the OH radical and Ar atoms. The frozen core approximation [MP2(FC)] and the aug-cc-pVTZ basis set were employed in all calculations. Basis-set superposition errors (BSSEs) were not included. It is expected that they are quite small at this theoretical level. The MP2 calculations were carried out with the Gaussian98 program [24].

The potentials describing the interaction between the OH radical and Ar are presented in Figures 1–3. In general, they are well represented by a 12-6 Lennard-Jones (LJ) model. The potential model for the interaction between hydrogen and Ar is presented in Figure 1. It shows a minimum of −0.00012 hartree (−0.075 kcal/mol) at $r = 6.5$ au. The model for the interaction between oxygen and Ar is presented in Figure 2. It shows a minimum of −0.0004 hartrees (−0.25 kcal/mol) at $r = 6.2$ au. These small values for the well depths indicate that the interactions between the OH radical and the Ar atoms are dominated by repulsive contributions. Figure 3 shows the interaction between the OH

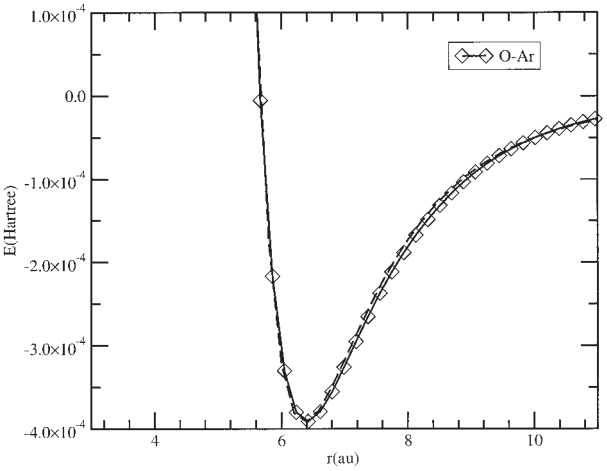

FIGURE 2. O—Ar interaction potential. UMP2/aug-cc-pVTZ calculations (diamonds) and fitted 12-6 Lennard-Jones potential (dashed curve).

radical and the Ar atom in a linear configuration where the Ar atom is at a distance r from the OH hydrogen. Quite interestingly, a shift to lower r values (≈5.2 au) is observed for the H—Ar interaction in the radical in comparison with free hydrogen (6.5 au). This reflects some polarization of the OH radical in interaction with Ar. This effect can be assessed by comparing the free radical and the OH—Ar complex charge distributions.

Data for the optimized structure, frequency, dipole moment, and binding energy for the OH—Ar complex are reported in Table I, where results for the free radical are also reported. The binding energy of the OH—Ar complex is 0.78 kcal/mol, which means a very weak attractive interaction. Consequently, our results do not support the view that hydrogen bonding and charge transfer are relevant to explain the structure of OH—Ar complexes [11]. The ν(O—H) frequency is red-shifted by 31 cm^{-1} in the complex relative to the free radical. Comparison between the dipole moments of OH (1.76 D) and OH—Ar (1.94 D) confirms some polarization of the radical due to the presence of Ar. To introduce, at least partially, polarization effects, the charge distribution of the OH radical in Ar will be represented by the charge distribution of the OH radical in interaction with Ar. In addition, we will assume explicitly that the Ar atoms are polarized by the OH radical charge distribution. This means that although our model is based on the O—Ar and H—Ar LJ pair potentials, an additional contribution due to induction interactions U_{ind} will be included, according to the expression

TABLE I

Data for OH and OH—Ar complex from MP2/aug-cc-pVTZ calculations.

	OH	OHAr
r(O—H)	1.831	1.832
r(H—Ar)		5.099
$\nu_{\text{O—H}}$	3795 (3738)[a]	3764
μ	1.76 (1.66)[b]	1.939
BE		0.78

Distances in atomic units. Frequencies (cm^{-1}) calculated at MP2/aug-cc-pVDZ. Dipoles in D. Binding energy (BE) in kcal/mol.

[a] Experimental value from Herzberg [8].

[b] Experimental value from Nelson et al. [27].

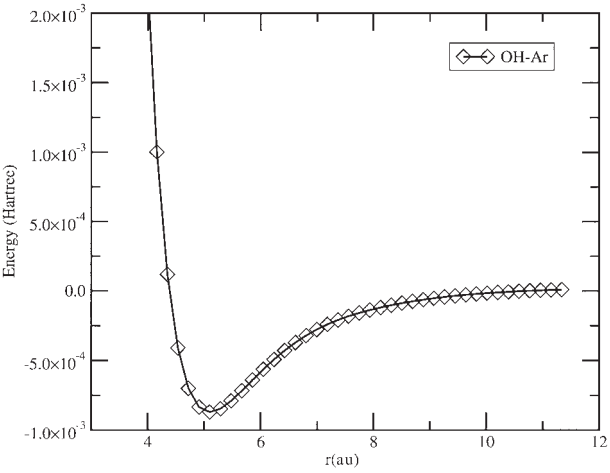

FIGURE 3. OH—Ar interaction potential for the linear complex. UMP2/aug-cc-pVTZ calculations.

$$U_{\text{ind}} = -1/2 \sum_j \sum_{\alpha,\beta} \alpha_{\alpha\beta} F^j_\alpha F^j_\beta, \tag{14}$$

where the field produced by the OH radical charges on the Ar atom j is

$$F^j_\alpha = \sum_{k \in \text{OH}} q_k T_\alpha(kj) \tag{15}$$

and

$$T_\alpha(kj) = R_\alpha(kj)/|R(kj)|^3. \tag{16}$$

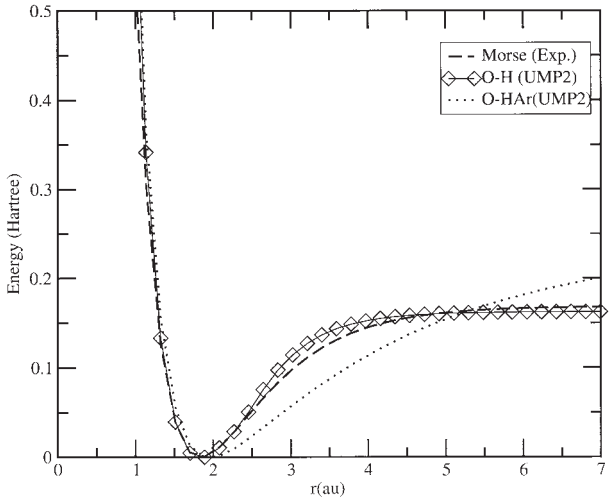

FIGURE 4. Morse potential for the OH radical. Experimental (dashed curve), UMP2/aug-cc-pVTZ calculations (diamonds). The dotted line is the O—H potential in the OH—Ar complex.

The average polarization of the Ar atoms $\alpha = (\alpha_{xx} + \alpha_{yy} + \alpha_{zz})/3 = 11.08$ (au)^3 [26]. It is known that induced interactions are not pairwise additive and that the final charge distribution in a polarizable system should be self-consistently determined [25]. However, in the present case, this contribution is quite small (although not negligible) and the following approximation was adopted: the polarizing field is only related to the OH charges and the interactions between the induced dipoles in the Ar atoms were neglected.

The experimental Morse potential describing the vibrational motion of the free OH radical [8] is reported in Figure 4. The same figure shows the potential based on UMP2/aug-cc-pVTZ calculations for the free radical (diamonds) and the curve corresponding to the vibrational motion of the OH radical coupled to one Ar atom (dotted curve). A good agreement between the experimental and the theoretical potential is observed, which supports the adequacy of the present approach. The presence of the Ar atom modifies the O—H vibrational degree of freedom introducing an attractive contribution from the minimum position, which remains nearly the same (1.9 au) up to 5 au, where a repulsive contribution due to the H—Ar interaction appears. The H—Ar distance was optimized for each O—H value. The full set of interaction and Morse potential parameters is reported in Table II.

OH Radical in Solid Argon

To model the vibrational structure of the OH radical in solid phase, we initially carried out conventional Monte Carlo simulations for the OH radical at its equilibrium distance (1.837 au) in the Ar matrix. The NPT ensemble was employed in a cubic cell with 108 Ar atoms and periodic boundary conditions. The interactions were truncated at 12 au. A preferential sampling algorithm for the atoms closer to the radical was used [28]. By using an annealing procedure, 4 million steps were carried out to equilibrate the system. The final configuration from the classical simulation at $T = 10$ K was at a reduced density $\rho^* = (N/V)\sigma^3 = 1.1$ and at a reduced temperature $T^* = k_B T/\epsilon = 0.083$, where ϵ and σ are Lennard-Jones parameters for Ar (see

TABLE II
Lennard–Jones and Morse potential parameters.

	O	H	Ar
Lennard-Jones $V_{LJ}(r)$[a]			
ϵ	4.048×10^{-4}	3.713×10^{-5}	3.793×10^{-4}
σ	4.874	6.009	6.462
Morse potential $V_M(r)$[b]			
D_e	0.1683		
α	1.2196		
r_e	1.8342		

Data in atomic units.
[a] $V_{LJ}(r) = 4\epsilon[(\sigma/r)^{12} - (\sigma/r)^6]$. Parameters fitted to UMP2/aug-cc-pVTZ calculations. Lorentz–Berthelot composition rules $\epsilon_{ij} = (\epsilon_i\epsilon_j)^{1/2}$ and $\sigma_{ij} = (\sigma_i + \sigma_j)/2$ were adopted.
[b] $V_M(r) = D_e[1 - \exp(-\alpha(r - r_e))^2]$. Parameters for OH $X^2\Pi$ from Herzberg [8].

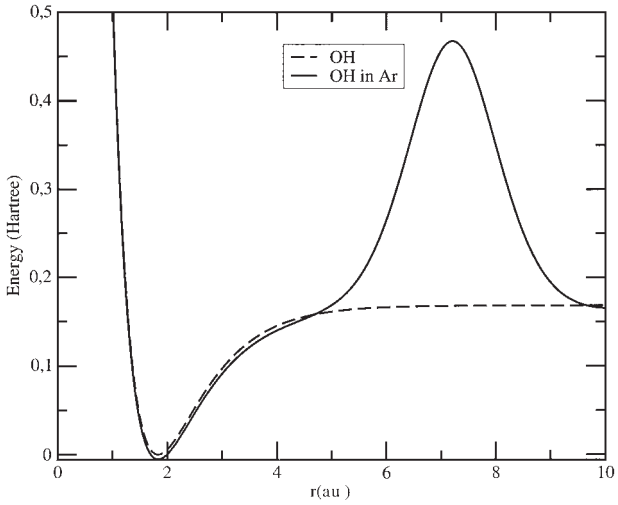

FIGURE 5. Morse potential for the free OH radical (dashed curve) and the effective potential for the OH in solid Ar.

Table II). From this configuration we started to generate new configurations in the NVT ensemble according to expression (5). The system was then equilibrated during 5000 steps and final averages correspond to additional 8000 steps. We note that no Monte Carlo sampling of the fast variable r is needed; in the present approach it is explicitly integrated. We observe the relatively small number of configurations for the mixed quantum-classical system. However, we believe that it is an acceptable number of steps (considering the large computational time) for the simulation in a matrix where small fluctuations should be expected.

Figure 5 shows the Morse potential describing the free OH vibrations and the effective averaged vibrational potential in solid Ar. From the minimum position up to ~5 au, the weak attractive interactions of the OH radical with the Ar matrix introduces a small shift to lower energies. This effect is small and the shape of the curve up to this distance (~5 au) is essentially the same, which is a clear indication of a modest condensed phase effect on the lower vibrational levels of the OH radical. However, in contrast with the vibrational behaviour for the free radical, the present results show that confinement effects due to repulsive interactions with the matrix will certainly modify the vibrational structure the OH radical. First, an energy barrier (~0.3 ± 0.15 au) above the free OH radical dissociation limit appears. In addition, new discretized vibrational levels will be present, indicating significant changes on the absorption spectra of OH, a feature already observed for Br_2 in solid Ar [23].

The changes on the vibrational structure can be illustrated by calculating $\Delta G_{v+1/2} = G(v + 1) - G(v)$. This quantity is reported in Figure 6 for the Morse O—H oscillator and for the O—H radical in Ar. For the free species, only two regimes exist. The first is a linear behavior typical of Morse oscillators, although it is not always observed in diatomic molecules, as, for example, H_2 [8]. The second regime correspond to continuum states levels. For OH in Ar, three regimes can be defined. The first, which involves the 12 lower vibrational levels is a Morse-like regime. The second is a transition regime, which deviates considerably from Morse and involves discrete vibrational levels from $v = 13$ up to $v = 20$. Finally, a third regime characterized by a nearly constant spacing between the vibrational levels (typical of harmonic regimes) is observed, which reflects confinement effects. We predict that in solid Ar, $\Delta G_{1/2} = G(1) - G(0) = 3540$ cm^{-1}, which is 8.2 cm^{-1} lower than the experimental value (3548.2 cm^{-1}) [12]. Thus, significant condensed phase effects on the vibrational structure of the OH radical should be expected, mainly if higher energy vibrational levels are involved. However, the effect is essentially related to confinement. At-

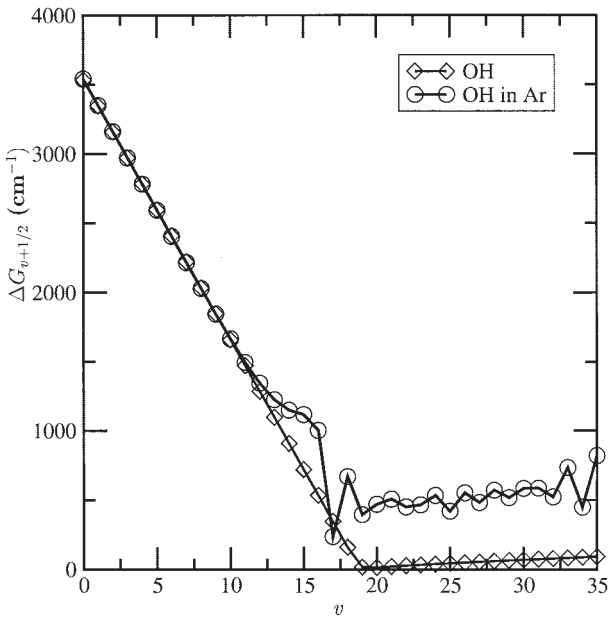

FIGURE 6. $\Delta G_{v+1/2} = G(v + 1) - G(v)$ for the OH Morse oscillator (diamonds) and for the oscillator in solid Ar (circles).

tractive interactions between the OH radical and the Ar atoms are weak and apparently play a minor role.

Conclusions

The vibrational structure of the OH radical in solid Ar was investigated by a transfer-matrix path-integral (TMPI) method previously proposed for mixed quantum-classical systems [23]. MP2 calculation for the OH—Ar complex indicates that the interaction between the radical and the Ar atom is very weak and amounts to less than 1 kcal/mol. Gas-phase calculations for the OH vibrational degree of freedom coupled to an Ar atom show that attractive short-range interactions are slightly enhanced. A repulsive contribution starting at ~5 au increases the dissociation energy relative to the free radical by ~0.04 hartree. TMPI calculations for the oscillator coupled to the Ar matrix indicates that the lower vibrational levels of the OH radical are not significantly modified relative to the gas phase, which is in agreement with the most recent experimental results [12]. The major changes concern higher vibrational levels (above $v = 12$), which is essentially a consequence of repulsive interactions and/or confinement effects. The calculations also indicate that the dissociation energy in solid Ar is increased by ≈0.3 hartree (188 kcal/mol) relative to the gas-phase value. However, in contrast with previous results for Br_2 in Ar [23], which indicated that strong confinement effects inhibited dissociation of the Br_2 molecule in the matrix, the results suggest that the OH radical can dissociate in solid Ar. In this sense, it appears that the present study based on TMPI may provide valuable information on bond-breaking processes in condensed phases.

ACKNOWLEDGMENTS

The author gratefully acknowledges the support of the Fundação para a Ciência e a Tecnologia (FCT) through project POCTI/43315/QUI/2001.

References

1. Haliwell, B.; Gutteridge, J. H. C. Free Radicals in Biology and Medicine; Oxford University Press: Oxford, 1989.
2. Kopenol, W. H. Free Radical Biol Med 1991, 10, 85.
3. Stadtman, E. R. Annu Rev Biochem 1993, 62, 797.
4. Aydogan, B.; Marshall, D. T.; Swarts, S. G.; Turner, J. E.; Boone, A. J.; Richards, N. G.; Bolch, W. E. Radiat Res 2002, 157, 38.
5. Linert, W.; Jameson, G. N. L. J Inorg Biochem 2000, 79, 319.
6. Chandra, A. K.; Uchimaru, T. J Phys Chem A 2000, 104, 8535.
7. Smith, I. W. M.; Ravishankara, A. R. J Phys Chem A 2002, 106, 4798.
8. Herzberg, G. Spectra of Diatomic Molecules; Van Nostrand: New York, 1950.
9. Herzberg, G. The Spectra and Structure of Simple Free Radicals; Dover: New York, 2003.
10. Acquista, N.; Schoen, L. J.; Lide, D. R. J Chem Phys 1968, 48, 1534.
11. Goodman, J.; Brus, L. E. J Chem Phys 1977, 67, 4858.
12. Cheng, B.-M.; Lee, Y.-P.; Ogilvie, J. F. Chem Phys Lett 1988, 151, 109.
13. Suzer, S.; Andrews, L. J Chem Phys 1988, 88, 916.
14. Langford, V. S.; McKinley, A. J.; Quickenden, T. I. J Am Chem Soc 2000, 122, 12859.
15. Engdahl, A.; Karlström, G.; Nelander, B. J Chem Phys 2003, 118, 7797.
16. Cooper, P. D.; Kjaergaard, H. G.; Langford, V. S.; McKinley, A. J.; Quickenden, T. I.; Schofield, D. P. J Am Chem Soc 2003, 125, 6048.
17. do Couto, P. C.; Guedes, R. C.; Costa Cabral, B. J.; Martinho Simões, J. A. J Chem Phys 2003, 119, 7344.
18. Herman, M. F.; Berne, B. J. Chem Phys Lett 1981, 77, 163.
19. Herman, M. F.; Berne, B. J. J Chem Phys 1983, 78, 4103.
20. Kramers, H. A.; Wannier, G. H. Phys Rev 1941, 60, 252.
21. Feynman, R. P. Statistical Mechanics; Benjamin: Reading, MA, 1972.
22. Ramalho, J. P. P.; Fernandes, F. M. S. Z Naturforsch A 1990, 45, 1193.
23. Ramalho, J. P. P.; Costa Cabral, B. J.; Fernandes, F. M. S. S. Chem Phys Lett 1991, 184, 53.
24. Frisch, M. J.; Trucks, G. W.; Schlegel, H. B.; Scuseria, G. E.; Robb, M. A.; Cheeseman, J. R.; Zakrzewski, V. G.; Montgomery, J. A.; Stratman, R. E.; Burant, J. C.; Dapprich, S.; Millan, J. M.; Daniels, A. D.; Nudin, K. N.; Strain, M. C.; Farkas, O.; Tomasi, J.; Barone, V.; Cossi, M.; Cammi, R.; Mennucci, B.; Pomelli, C.; Adamo, C.; Clifford, S.; Ochterski, J.; Peterson, G. A.; Ayala, P. Y.; Cui, Q.; Morokuma, K.; Malick, D. K.; Rabuck, A. D.; Raghavachari, K.; Foresman, J. B.; Cioslowski, J.; Ortiz, J. V.; Stefanov, B. B.; Liu, G.; Liashenko, A.; Piskorz, P.; Komaromi, I.; Gomperts, R.; Martin, R. L.; Fox, D. J.; Keith, T.; Al-Laham, M. A.; Peng, C. Y.; Nanayakkara, A.; Gonzalez, C.; Challacombe, M.; Gill, P. M. W.; Johnson, B. G.; Chen, W.; Wong, M. W.; Andres, J. L.; Head-Gordon, M.; Repogle, E. S.; Pople, J. A. GAUSSIAN-98; Gaussian Inc.: Pittsburgh, PA, 1998.
25. Costa Cabral, B. J.; Rivail, J. L.; Bigot, B. J Chem Phys 1987, 86, 1467.
26. Gray, C. G.; Gubbins, K. E. Theory of Molecular Fluids; Clarendon: Oxford, 1984.
27. Nelson, R. D., Jr.; Lide, D. R.; Maryott, A. A. Selected Values of Electric Dipole Moments for the Molecules in the Gas Phase; NSRDS-NBS10; National Bureau of Standards: Washington, DC, 1967.
28. Owicki, J. C.; Scheraga, H. A. J Am Chem Soc 1977, 99, 7403.